# Quantitative molecular sensing in biological tissues: an approach to non-invasive optical characterization

**Malavika Chandra[*1], Karthik Vishwanath[*2], Greg D. Fichter[3], Elly Liao[2], Scott J. Hollister[2,4,5], and Mary-Ann Mycek[1,2]**

*Applied Physics Program[1] and Depts. of Biomedical Engineering[2], Electrical Engineering and Computer Science[3], Surgery[4], and Mechanical Engineering[5], University of Michigan, Ann Arbor, MI 48109-2099*
mycek@umich.edu

** These authors contributed equally to this work.*

**Abstract:** A method to non-invasively and quantitatively characterize thick biological tissues by combining both experimental and computational approaches in tissue optical spectroscopy was developed and validated on fifteen porcine articular cartilage (AC) tissue samples. To the best of our knowledge, this study is the first to couple non-invasive reflectance and fluorescence spectroscopic measurements on freshly harvested tissues with Monte Carlo computational modeling of time-resolved propagation of both excitation light and multi-fluorophore emission. For reflectance, quantitative agreement between simulation and experiment was achieved to better than 11%. Fluorescence data and simulations were used to extract the ratio of the absorption coefficients of constituent fluorophores for each measured AC tissue sample. This ratio could be used to monitor relative changes in concentration of the constituent fluorophores over time. The samples studied possessed the complexity and variability not found in artificial tissue-simulating phantoms and serve as a model for future optical molecular sensing studies on tissue engineered constructs intended for use in human therapeutics. An optical technique that could non-invasively and quantitatively assess soft tissue composition or physiologic status would represent a significant advance in tissue engineering. Moreover, the general approach described here for optical characterization should be broadly applicable to quantitative, non-invasive molecular sensing applications in complex, three-dimensional biological tissues.



**OCIS codes:** (170.6510) Spectroscopy, tissue diagnostics; (170.3650) Lifetime-based sensing; (170.3660) Light propagation in tissues

## References and links

1. B. Wilson, and S. Jacques, "Optical reflectance and transmittance of tissues: principles and applications," IEEE J. Quantum Electron. **26**, 2186-2199 (1990).
2. I. Bigio, and J. Mourant, "Ultraviolet and visible spectroscopies for tissue diagnostics: fluorescence spectroscopy and elastic-scattering spectroscopy," Phys. Med. Biol. **42**, 803-814 (1997).
3. S. Andersson-Engels, C. Klinteberg, K. Svanberg, and S. Svanberg, "In vivo fluorescence imaging for tissue diagnostics," Phys. Med. Biol. **42**, 815-824 (1997).
4. R. Richards-Kortum, and E. Sevick-Muraca, "Quantitative optical spectroscopy for tissue diagnosis," Annu. Rev. Phys. Chem. **47**, 555-606 (1996).
5. M.-A. Mycek, and B. W. Pogue, eds., *Handbook of Biomedical Fluorescence* (Marcel Dekker, Inc., New York, 2003).
6. V. Backman, M. B. Wallace, L. T. Perelman, J. T. Arendt, R. Gurjar, M. G. Müller, Q. Zhang, G. Zonios, E. Kline, T. McGillican, S. Shapshay, T. Valdez, K. Badizadegan, J. M. Crawford, M. Fitzmaurice, S.

#69865 - $15.00 USD Received 10 April 2006; revised 24 May 2006; accepted 4 June 2006

Kabani, H. S. Levin, M. Seiler, R. R. R. R. Dasari, I. I. Itzkan, J. J. Van Dam, and M. S. Feld, "Detection of preinvasive cancer cells," Nature **406**, 35-36 (2000).
7. K. T. Schomacker, J. K. Frisoli, C. C. Compton, T. J. Flotte, J. M. Richter, and T. F. Deutsch, "Ultraviolet laser-induced fluorescence of colonic polyps," Gastroenterology **102**, 1155-1160 (1992).
8. N. Ramanujam, M. F. Mitchell, A. Mahadevan, S. Warren, S. Thomsen, E. Silva, and R. Richards-Kortum, "In vivo diagnosis of cervical intraepithelial neoplasia using 337-nm-excited laser-induced fluorescence," in *Proceedings of the National Academy of Science, USA*, **91**, 10193-10197 (1994).
9. M.-A. Mycek, K. Schomacker, and N. Nishioka, "Colonic polyp differentiation using time resolved autofluorescence spectroscopy," Gastrointest. Endosc. **48**, 390-394 (1998).
10. J. R. Lakowicz, *Principles of Fluorescence Spectroscopy* (Kluwer Academic/Plenum, New York, 1999).
11. S. Chandrasekhar, *Radiative Transfer* (Dover, N.Y., 1960).
12. J. Wu, M. Feld, and R. Rava, "Analytical model for extracting intrinsic fluorescence in turbid media," Appl. Opt. **32**, 3585-3595 (1993).
13. M. S. Patterson and B. W. Pogue, "Mathematical model for time-resolved and frequency-domain fluorescence spectroscopy in biological tissues," Appl. Opt. **33**, 1963-1974 (1994).
14. W. M. Star, J. P. A. Marijnissen, and M. J. C. van-Gemert, "Light Dosimetry in optical phantoms in tissues: I. Multiple flux and transport theory," Phys. Med. Biol **33**, 437-454 (1988).
15. A. J. Welch, and M. J. C. van-Gemert, *Optical-Thermal Response of Laser-Irradiated Tissue* (Plenum Press, New York, 1995), Chap. 4, 9.
16. G. Zonios, R. Cothren, J. Arendt, J. Wu, J. Van Dam, J. Crawford, R. Manoharan, and M. Feld, "Morphological model of human colon tissue fluorescence," IEEE Trans. Biomed. Eng. **43**, 113-122 (1996).
17. H. Zeng, C. MacAulay, D. I. McLean, and B. Palcic, "Reconstruction of in vivo skin auto fluorescence spectrum from microscopic properties by Monte-Carlo simulation," J. Photochem. Photobiol. B **38**, 234-240 (1997).
18. B. Pogue, and T. Hasan, "Fluorophore quantitation in tissue simulating media with confocal detection," IEEE J. Sel. Top. Quantum Electron. **2**, 959-964 (1996).
19. K. Vishwanath, and M.-A. Mycek, "Do fluorescence decays remitted from tissues accurately reflect intrinsic fluorophore lifetimes?," Opt. Lett. **29**, 1512-1514 (2004).
20. K. Vishwanath, and M.-A. Mycek, "Time-resolved photon migration in bi-layered tissue models," Opt. Express **13**, 7466-7482 (2005).
21. J. A. Buckwalter, and H. J. Mankin, "Instructional course lectures, The American Academy of Orthopaedic Surgeons-Articular Cartilage. Part I: Tissue Design and Chondrocyte-Matrix Interactions," J. Bone and Jt. Surg. (American) **79**, 600-611 (1997).
22. J. D. Pitts and M.-A. Mycek, "Design and development of a rapid acquisition laser-based fluorometer with simultaneous spectral and temporal resolution.," Rev. Sci. Instrum. **72**, 3061-3072 (2001).
23. D. Y. Churmakov, I. V. Meglinski, S. A. Piletsky, and D. A. Greenhalgh, "Analysis of skin tissues spatial fluorescence distrubution by the Monte Carlo simulation," J. Physics D: Appl. Phys. **36**, 1722-1728 (2003).
24. L. Lindqvist, B. Czochralska, and I. Grigorov, "Determination of the mechanism of photo-ionization of NADH in aqueous solution on laser excitation at 355 nm," Chem. Phys. Lett. **119**, 494-497 (1985).
25. S. A. Prahl, M. J. C. van Gemert, and A. J. Welch, "Determining the optical properties of turbid media by using the adding-doubling method," Appl. Opt. **32**, 559-568 (1993).
26. S. A. Prahl, "Inverse Adding-Doubling," http://omlc.ogi.edu/staff/prahl.html.
27. K. Vishwanath, B. W. Pogue, and M.-A. Mycek, "Quantitative fluorescence lifetime spectroscopy in turbid media: comparison of theoretical, experimental and computational methods," Phys. Med. Biol. **47**, 3387-3405 (2002).
28. L. Wang, S. L. Jacques, and L. Zheng, "MCML-Monte Carlo modeling of photon transport in multi-layered tissues," Computer Methods and Programs in Biomedicine **47**, 131-146 (1995).
29. S. L. Jacques, "Time resolved propagation of ultrashort laser pulses within turbid tissue," Appl. Opt. **28**, 2223-2229 (1989).
30. K. Vishwanath, "Computational modeling of time-resolved fluorescence transport in turbid media for non-invasive clinical diagnostics",Ph.D. Thesis in *Applied Physics Program*, (University of Michigan, Ann Arbor), Chapter 3, Section 3.1, p 67,(2005).
31. J. F. Beek, P. Blokland, P. Posthumus, M. Aalders, J. W. Pickering, H. J. C. M. Sterenborg, and M. J. C. van Gemert, "In vitro double-integrating-sphere optical properties of tissues between 630 and 1064 nm," Phys. Med. Biol. **42**, 2255-2261 (1997).
32. R. Drezek, K. Sokolov, U. Utzinger, I. Boiko, A. Malpica, M. Follen, and R. Richards-Kortum, "Understanding contributions of NADH and collagen to cervical tissue fluorescence spectra: Modeling, measurements, and implications," J. Biomed. Opt. **6**, 385-396 (2001).
33. P. Å. Öberg, T. Sundqvist, and A. Johansson, "Asessment of cartilage thickness utilising reflectance spectroscopy," Med. Biol. Eng. Comput. **42**, 3-8 (2004).
34. L. Marcu, D. Cohen, J.-M. I. Maarek, and W. S. Grundfest, "Characterization of Type I, II, III, IV and V collagens by time-resolved laser-induced fluorescence spectroscopy," in *Optical Biopsy III*, R. R. Alfano, ed., Proc. SPIE **3917**, 93-101 (2000).
35. C. B. Talbot, R. K. P. Benninger, P. de Beule, J. Requejo-Isidro, D. S. Elson, C. Dunsby, I. Munro, M. A. Neil, A. Sandison, N. Sofat, H. Nagase, P. M. W. French, and M. J. Lever, "Application of hyperspectral

#69865 - $15.00 USD Received 10 April 2006; revised 24 May 2006; accepted 4 June 2006

fluorescence lifetime imaging to tissue autofluorescence: arthritis," in *Diagnostic Optical Spectroscopy in Biomedicine III*, M.-A. Mycek, ed., Proc. SPIE-OSA Biomedical Optics **5862**, 58620T (2005).

## 1. Introduction

Methods of optical spectroscopy and imaging are being developed for a variety of biomedical applications in non- or minimally-invasive tissue diagnostics, including sensing molecular concentrations of delivered pharmaceutical or contrast agents, probing tissue physiologic status, and detecting early stages of disease *in vitro* and *in vivo* [1-5]. In tissue optics, one of the challenges is to obtain quantitative information despite the detected signal variability introduced by tissue morphology and optical absorption and scattering.

The interaction of light with complex, inhomogeneous media such as tissue is characterized by a variety of processes that depend on the physical nature of the light and the specific morphology and composition of the tissue. Incident light may be scattered (elastically or inelastically) multiple times due to microscopic differences in the index of refraction within the tissue, it may be absorbed by fluorophores, which may then release their excess energy by radiative decay, producing fluorescence or be non-radiatively absorbed by chromophores present in the medium. The remitted fluorescent light may, in turn, be multiply scattered or absorbed. In biological tissues, reflected and fluorescent light reaching the tissue surface is affected by scattering (e.g., from inhomogeneities including extracellular matrix and membranes and intracellular nuclei and mitochondria) and absorption (e.g., from hemoglobin and proteins).

The goal of the study reported here was to develop and validate a method to non-invasively and quantitatively characterize thick biological tissues by combining both experimental and computational approaches in tissue optical spectroscopy. We developed and employed prototype instrumentation for reflectance and fluorescence spectroscopy that is compatible with both clinical and laboratory studies, as well as novel computational codes developed to model time-resolved excitation and fluorescent light propagation in multi-fluorophore biological tissues.

Reflectance spectroscopy can provide pathologically relevant information about living tissues, including tissue morphology, as well as the size, shape and, density of cells [1,2]. Such information can help track architectural changes in tissue and has been employed to study dysplasia in living tissue [6]. Fluorescence methods are useful in biomedical research for several reasons, including the molecular specificity of the technique, the relatively large signal strength in regions of the electromagnetic spectrum readily accessible to experimentalists, and the many bio-compatible fluorophores (endogenous and exogenous) available for study. Endogenous tissue fluorescence (autofluorescence) provides information about the native biochemical composition and microenvironment in living tissues without the use of contrast agents. Fluorescence spectroscopy may be performed with thin, flexible, fiber-optic probes; the technique is thus clinically feasible and allows access to internal organs endoscopically or surgically [5,7-9].

In contrast to steady-state (or, time-integrated) optical methods, time-resolved optical spectroscopy and imaging involves delivering a pulse of light to a sample under investigation and detecting the transient response of the medium in the time-domain. Steady-state fluorescence measurements integrate the signal over time, thus losing an additional dimension of information contained in the dynamics of the fluorescence decay. Fluorophore lifetimes are known to be sensitive to the local biochemical environment and to vary with pH and oxygenation in a controlled way, but are generally independent of artifacts influencing fluorescence intensity, including fluorophore concentration, photobleaching, and sources of optical loss (absorption and scattering) in biological systems [10]. This is an important issue to consider when applying fluorescence spectroscopy *in vivo*, since intensity losses attributed to hemoglobin absorption in tissue are routinely observed in the lineshape of the steady-state emission spectrum when measured *in vivo* [7,9]. Since biomolecules generally have broad and

#69865 - $15.00 USD Received 10 April 2006; revised 24 May 2006; accepted 4 June 2006

overlapping fluorescence spectral bands, lifetime spectroscopy can provide an alternate means of *in situ* discrimination in multi-fluorophore systems, including the tissues studied here.

In order to quantify optical measurements made in tissues, it is necessary to accurately describe all light-tissue interactions. Analytical treatment of light propagation in tissue is possible by considering light to be composed of neutral particles, and applying the radiative transport equation to describe photon propagation in such turbid media [11]. A common simplification to this approach has been to use the diffusion approximation to the radiative transport equation, which yields analytical solutions for the light energy distribution, both spatially and temporally, when applied to simple geometries [12-14]. The mathematical intractability and the assumptions of analytical approaches are significant and have limited the utility of the diffusion theory approximation in experiments on tissues that have multiple constituents or complex source configurations. A widely used technique for quantitative simulations of light-tissue interactions involves the use of Monte Carlo (MC) models for photon transport in turbid media, since they provide accurate predictions of light energy distribution in turbid media along with the ability to model complex tissue architectures and compositions, as well as source-detector geometries [5,15]. Although the MC model requires a prior knowledge of the medium's optical transport coefficients at wavelengths of interest, it has been shown to be an accurate model for the recovery of intrinsic fluorescence from tissue for both steady-state as well as time-resolved applications [15-20].

The work described here represents the first study to our knowledge to couple non-

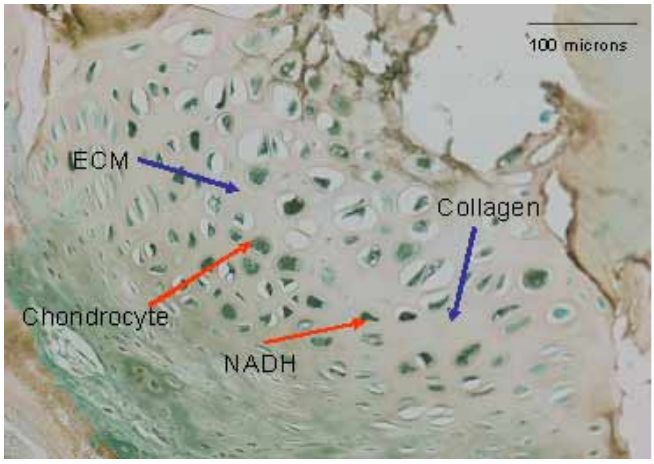


Fig. 1. Immunohistochemical staining for collagen type II (brown) found in the extracellular matrix (ECM) (blue arrows) of porcine knee articular cartilage (AC). Red arrows indicate cells (chondrocytes) where NADH is found.

invasive reflectance and fluorescence spectroscopic measurements on thick, fresh tissues with computational modeling of time-resolved photon propagation of both excitation light and multi-fluorophore emission, achieving agreement between simulation and experiment to better than 11% for reflectance. Fluorescence data and simulations were used to extract a quantitative measure to monitor relative changes in concentration of the constituent fluorophores in AC tissue over time. The porcine articular cartilage (AC) tissue samples studied offer the biologic variability not found in artificial tissue-simulating phantoms and serve as a model for future optical molecular sensing studies on tissue engineered AC constructs intended for use in human therapy. Tissue engineering is the process of creating functional biologic prostheses by suspending dissociated cells into biodegradable polymer scaffolds, which ultimately leads to new tissue formation. A significant challenge in tissue engineering is to assess non-invasively and quantitatively how engineered tissues compare to normal tissue. Most evaluation of soft tissue regeneration is done via histology, which is invasive, time-consuming, and inherently qualitative. An optical technique that could non-

#69865 - $15.00 USD Received 10 April 2006; revised 24 May 2006; accepted 4 June 2006

invasively and quantitatively determine soft tissue composition or cellular function would represent a significant advance in the assessment of engineered tissues. Moreover, the general approach described here, coupling experimental optical spectroscopy with computational modeling, should be broadly applicable to quantitative, non-invasive molecular sensing applications in complex, three-dimensional biological tissues.

## 2. Materials, instrumentation, and methods

### *2.1 Porcine knee articular cartilage (AC) sample preparation*

Hyaline AC is found in the synovial joints and is composed of chondrocytes surrounded by extracellular matrix, which is mainly composed of tissue fluid (80% water) and a macromolecular framework composed of collagens (mainly collagen type II, 90% – 95%), proteoglycans, and non-collagenous proteins and glycoproteins [21]. Figure 1 shows a micrograph of porcine knee AC tissue made by using an antibody based immunochemical stain (C7510-20F, United States Biological, Swampscott, MA) that specifically stains collagen type II in brown color. Cells and remaining tissue components not containing collagen type II appeared green in the figure.

Sixteen porcine knee AC samples (approximately 1-2 mm in thickness) were either freshly harvested (with measurements done 1-2 hours after harvesting) or cultured in culture media composed of dulbecco's modified eagle's medium (11995-065, Gibco/Invitrogen, Carlsbad, CA) + 10% fetal bovine serum (16000-044, Gibco/Invitrogen) + 1% penicillin/streptomycin (15140-122, Gibco/Invitrogen) for 1 week before measurements were taken. These two groups of samples were employed to determine whether culturing would affect tissue optical response. No marked differences were observed between the two groups. All samples were washed in phosphate-buffered saline (Cat. No.110010-023, Invitrogen) to remove traces of blood and cell culture media, placed on 0.88 mm thick quartz microscope slides (01018-AB, Structure Probe Inc., West Chester, PA) and sealed inside imaging chamber gaskets (C-18160, Invitrogen) for experimental measurements. Two of the samples (cultured) were used to extract tissue scattering and absorption coefficients via integrating sphere measurements. The remaining fourteen samples were employed for steady-state and time-resolved fluorescence measurements. Reflectance measurements were performed on eleven out of these fourteen samples and a fluorescence excitation-emission matrix (EEM) was acquired using one of the other three samples.

### *2.2 Spectrofluorimetry*

A spectrofluorometer (SPEX® FL3-22 Fluorolog-3, Jobin-Yvon Horiba, Japan) was employed to measure the EEM for AC tissue. The Fluorolog-3 spectrofluorometer was equipped with a 450 W Xe short arc lamp source that was focused onto a tunable, double excitation spectrometer (Czerny-Turner 1200/mm kinematic grating blazed at 330 nm) to produce a monochromatic collimated excitation beam at the sample at any desired wavelength from 290-900 nm. Remitted fluorescence was collected perpendicular to the excitation direction, collimated, and dispersed by a tunable double emission spectrometer (Czerny-Turner 1200/mm kinematic grating blazed at 500 nm) into a multialkali photomultiplier tube detector. The system was interfaced to a computer via custom software which allowed an automated scanning of the sample via measurement of an excitation spectrum, an emission spectrum, or combined EEM spectra. The AC sample was front illuminated to obtain the EEM for 25 excitation wavelengths between 320 and 450 nm while monitoring the emission between 340-650 nm (at 1 nm increments). Data acquisition time was approximately 6 minutes.

### *2.3 Reflectance, steady-state fluorescence and fluorescence lifetime spectrometer*

A portable Reflectance and Fluorescence Lifetime Spectrometer (RFLS) (Fig. 2) was employed to study AC tissues. For fluorescence excitation, the RFLS employed a pulsed, solid-state laser source (PNV001525-140, JDS Uniphase, San Jose, CA) with an adjustable

#69865 - $15.00 USD Received 10 April 2006; revised 24 May 2006; accepted 4 June 2006

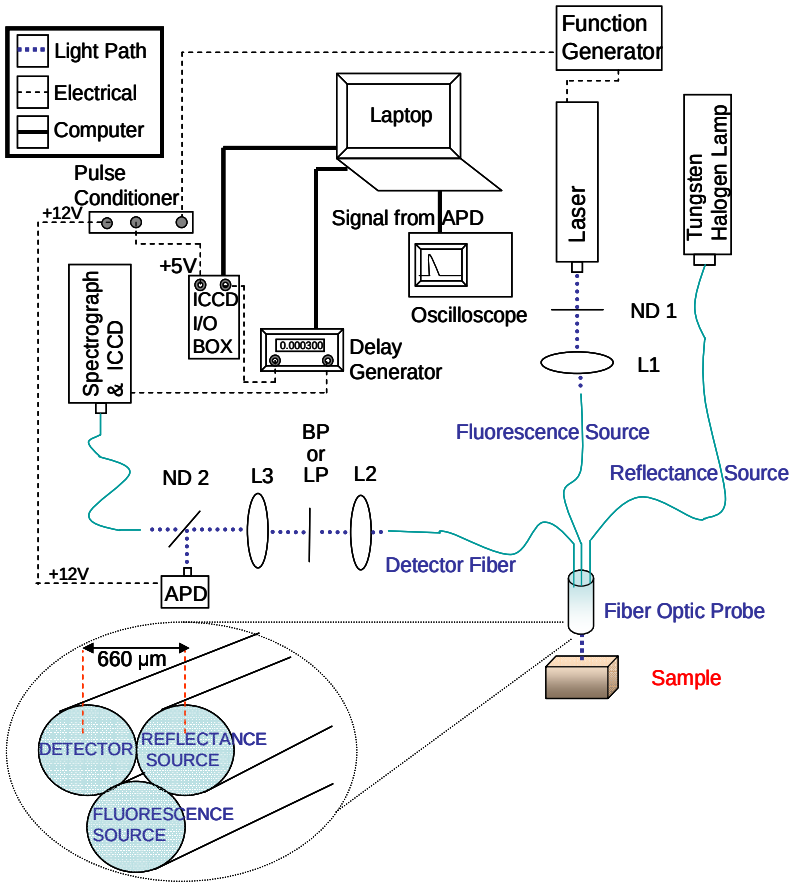


Fig. 2. Schematic of the Reflectance and Fluorescence Lifetime Spectrometer (RFLS) (ND – neutral density filter, L – lens, LP – long-pass filter, BP- band-pass filter, APD – avalanche photo diode, ICCD – intensified charge coupled device). The inset shows a schematic of the geometry of the fiber optic probe.

repetition rate (1- $10^3$ Hz) emitting at 355 nm with a 500 ps pulse width and an energy of 15 µJ/pulse. A function generator (33220A, Agilent, Palo Alto, CA) was employed to trigger the laser. After attenuating pulse energy with a neutral density (ND) filter (ND1), laser light was delivered to the sample via an optical fiber (fluorescence source fiber) (SFS600/660N, Fiberguide Industries, Stirling, NJ) of 600 µm core diameter and 0.22 numerical aperture (NA). For reflectance measurements, light from a tungsten halogen lamp (HL 2000FHSA, Ocean Optics, Dunedin, FL) with continuous wave (CW) output between 360-2000 nm was delivered to the sample by a second identical optical fiber (reflectance source fiber). At the distal end, the fiber probe was comprised of these two source fibers and a third, identical detector fiber placed adjacent to each other in a triangular geometry (Fig. 2, inset). Fluorescence and reflectance measurements were taken sequentially.

For fluorescence measurements, the emitted signal was collected by the detector fiber and focused by a series of lenses (L2 and L3) before reaching the detectors. The excitation light was eliminated at this stage by placing a long-pass (LP) filter that cut on at 387 nm (LP 57345, Spectra Physics, Mountain View, CA). A portion of the fluorescence was split off by a ND filter (ND2) and directed towards an avalanche photodiode (APD) (C5658, Hamamatsu, Bridgewater, NJ). The time-resolved signal detected by the APD was sampled at 4 MHz by a digitizing oscilloscope (TDS 784A , Tektronix, Beaverton, OR) and the data was recorded using software written in Labview (Labview 7.1, National Instruments, Austin, TX). The rest

#69865 - $15.00 USD Received 10 April 2006; revised 24 May 2006; accepted 4 June 2006

of the fluorescence was sent to a spectrograph (MS 125, Oriel Instruments, Stratford, CT) coupled intensified charge coupled device (ICCD) camera (ICCD 2063, Andor Technology, Belfast, Northern Ireland) for spectral data detection. To minimize background signal, the ICCD gating was synchronized with the arrival of the fluorescence signal. To do this, a part of the trigger signal to the laser was fed to a home built pulse conditioner (described previously [22]), which provided a stable TTL pulse output. This TTL pulse was then fed to a delay generator (DG535, Stanford Research Systems, Sunnyvale, CA) that introduced a 144 μs delay in the ICCD gate (4 μs gate width) with respect to the triggering of the laser.

For reflectance measurements, the LP and ND2 filters were removed and the optical signal from the sample was sent via the detector fiber and focusing optics directly to the spectrograph-coupled ICCD camera. The ICCD camera was run in its internal mode (i.e. the gate was open throughout data acquisition) and room lights were turned off to minimize background signal.

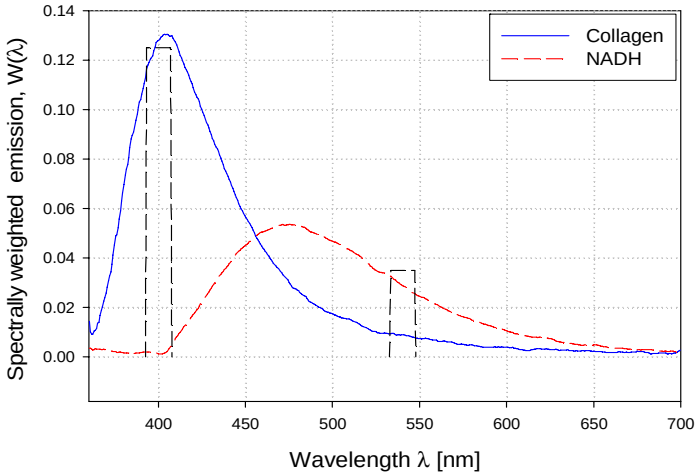


Fig. 3. Spectrally weighted fluorescence emission *W(λ)* (see text) for two fluorophores in the AC tissue. These spectra were measured on the RFLS for powdered collagen II (blue line) and for 70 μM NADH in DI-$H_2O$ (red dashed line). The black dashed lines indicate the spectral position of band-pass filters that were employed for obtaining time-resolved fluorescence measurements from porcine AC samples.

For fluorescence and reflectance measurements, a background spectrum was acquired with the sources blocked and was subtracted from the detected sample spectrum. Background subtracted data were then corrected to give distortion free spectra in units of photon numbers by calibrating the wavelength and correcting for the spectral instrument response of the RFLS. Details of these calibration procedures were described earlier [22]. Reflectance spectra were also corrected for the intensity spectrum of the lamp. First, the lamp spectrum was measured by placing a ND filter of OD 0.03 (03FNQ002, Melles Griot, Rochester, NY) in lieu of the tissue sample. Next, the background subtracted (instrument response corrected and normalized) tissue sample reflectance spectrum ($R_{sample}$) was divided by the background subtracted (instrument response corrected and normalized) lamp spectrum ($R_{lamp}$), to give the normalized reflectance spectrum (R) from each AC tissue sample (i.e. $R = R_{sample} / R_{lamp}$).

In this study, all measurements were taken with the fiber optic probe oriented normal to, and at a slight distance (0.5-1.0 cm) above, the AC tissue surface to mimic likely experimental conditions for studies on sterile samples. Reflectance spectra were measured keeping the ICCD gate open for 380 μs and steady-state fluorescence spectra were measured by averaging over 1600 pulses (1.6 s integration time), as described above. For fluorescence measurements, laser pulse energy was attenuated using an ND1 filter of optical density (OD) 1.0 (03FNQ015,

#69865 - $15.00 USD Received 10 April 2006; revised 24 May 2006; accepted 4 June 2006

Melles Griot). Three set of time-resolved fluorescence measurements were made on each sample: one full spectrum measurement (using the LP filter) and two wavelength-selected measurements (using BP filters (centered at 400 and 540 ± 10 nm) in place of the LP filter). All time-resolved fluorescence measurements were collected by averaging over 50 pulses. All measured fluorescence decays $M(t)$ were interpreted as a convolution of the intrinsic fluorescence decay, $f(t)$, and the instrument response function, $I(t)$: i.e. $M(t) = f(t) \otimes I(t)$ [22], where $f(t)$ was modeled as a double exponential decay: $f(t) = \sum c_i \exp(-t/\tau_i)$, ($i$ = 1,2) because the AC tissue was considered to be composed of a long-lived (collagen) and a short-lived (NADH) fluorophore. The average decay time $\tau$, was calculated as $\tau = [(c_{1*} \tau_1^2 + c_{2*} \tau_2^2)/ (c_{1*} \tau_1 + c_{2*} \tau_2)]$.

Figure 3 shows the spectral positions of the BP filters (black dashed lines) relative to the spectrally weighted fluorescence emission $W(\lambda)$ of collagen (blue line, solid) and NADH (red line, dashed). These fluorescence emission spectra were acquired on the RFLS from NADH (N-8129, Sigma Aldrich, St. Louis, Missouri) in DI-$H_2O$ (70 µM) and collagen type II (C-1188, Sigma Aldrich) in powder form. In order to calculate $W(\lambda)$ each measured fluorescence spectrum was normalized by setting the maximum fluorescence emission intensity to unity (thus getting rid of fluorophore concentration effects), then scaled such that area under each curve was unity, and finally multiplied by the quantum yield ($\Phi_{QY}$) of the corresponding fluorophore (0.15 for collagen and 0.1 for NADH obtained from literature [19,23,24]). As seen in Fig. 3, at BP 400 nm, collagen dominated the fluorescence emission relative to NADH, while at BP 540 nm, this was reversed. Thus, the effects of the changes in the measured fluorescence decays from a medium containing these two fluorophores (NADH and Collagen II), obtained via these two BP filters could be quantitatively modelled using a Monte Carlo model (described below in Section 2.5).

*2.4 Integrating sphere measurements*

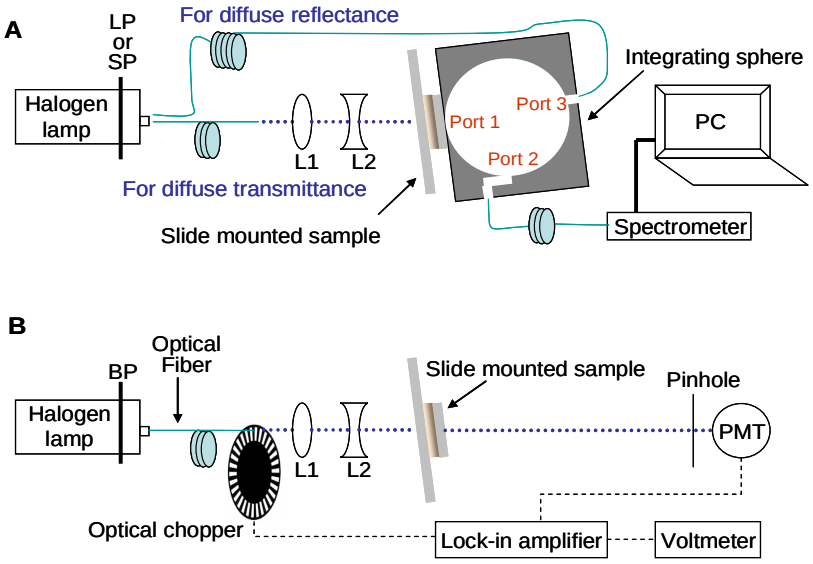


Fig. 4. (a) Schematic for diffuse reflectance and transmittance measurements using an integrating sphere. (b) Schematic for collimated transmittance measurements. (L- Lens; LP – long-pass filter; SP – short-pass filter; BP – band-pass filter; PMT – photomultiplier tube; Port 1 – sample port; Port 2 – detection port; Port 3 – reflectance port).

Tissue scattering and absorption coefficients ($\mu_s$ and $\mu_a$, respectively) were determined using an integrating sphere (IS) and the inverse adding-doubling (IAD) method [25]. The adding-doubling method models random scattering events in a planar sample by approximating the

#69865 - $15.00 USD Received 10 April 2006; revised 24 May 2006; accepted 4 June 2006

sample as a discrete number of scattering layers and scattering angles. The IAD method used iteration to fit the measurements, and was implemented using IAD software available online [26]. The method required separate measurements of diffuse reflectance, diffuse transmittance, and collimated transmittance as illustrated in Fig. 4. A CW tungsten halogen lamp (LS-1, Ocean Optics) emitting light between 360-2000 nm with a 200 micron fiber coupling was used for all measurements.

Two cultured AC tissue samples, each with overall thickness 1.2 mm, were measured. For diffuse reflectance measurements, the light source was attached to the reflectance port (Port 3) of an integrating sphere (Avasphere-30, Avantes, Boulder, CO) [Fig. 4(a)]. The sample was placed at the sample port (Port 1, 8 mm diameter) and the collimated light formed a spot size approximately 5 mm in diameter on the sample. The sum of intensity of diffuse and specular reflected light was measured using a spectrometer (USB-2000, Ocean Optics) coupled to the IS with a 600 micron core fiber at the detection port (Port 2). Integration times varied from 4-60 seconds. Reflectance measurements were calibrated using a 75% reflectance standard (SRS-75-010, Labsphere, North Sutton, New Hampshire). Diffuse transmittance measurements [Fig. 4(a)] were taken by collimating the fiber coupled light source by a lens pair (L1 and L2) to form a spot size approximately 4 mm in diameter at the sample. For this measurement, the IS was tilted to prevent collimated transmitted light from falling on the uncoated portion of the sphere at the reflectance port. Two set of diffuse reflectance and transmittance spectra were taken - for source wavelengths less than, and greater than 420 nm - by placing appropriate filters (SP or LP) in front of the lamp. This reduced the number of photons hitting the spectrograph detector and avoided saturation of the detector.

For collimated transmittance measurements [Fig. 4(b)] the IS and spectrometer were removed and a photomultiplier tube (PMT) (R928, Hamamatsu) was employed for light detection. A pinhole placed in front of the PMT limited the acceptance angle to 0.17 degrees to eliminate fluorescent and diffuse light. An optical chopper (SR540, Stanford Research Systems) and lock-in amplifier (LIA-MV-150, Femto, Berlin, Germany) were employed to increase sensitivity. Measurements were taken for 9 wavelengths by placing narrowband (nominally 10 nm full width at half maximum) bandpass (BP) filters at the source (Table 1). Transmittance measurements were calibrated using ND filters of OD 1.0 (03FNQ015, Melles Griot) and OD 3.0 (03FNQ027, Melles Griot).

### *2.5 Monte Carlo model for photon migration simulations*

An MC transport code was used to simulate both time-resolved reflectance and fluorescence from an AC tissue model (Fig. 5). The AC tissue model was a bulk medium (0.12 cm thickness) containing two uniformly distributed fluorophores (intracellular NADH and collagen type II in the extracellular matrix). $2.5 \times 10^7$ photons were launched into the tissue model normal to the surface, at the air-tissue interface via a source optical fiber of specified numerical aperture (0.22) and diameter (600 microns core). Reflectance and fluorescence escaping the tissue per unit time was collected at surface within detector annuli concentric with the source fiber. The spacing between consecutive (detection) rings was identical and set equal to source fiber diameter. As described in detail previously [27], photon trajectories (black lines, Fig. 5) were constructed by stochastic sampling of scattering angles (specified by the anisotropy coefficient, $g$) and path lengths (specified by the scattering coefficient, $\mu_s$). Each photon entered the tissue medium with a weight of unity, which was attenuated exponentially as given by Beer's law for the absorption coefficient $\mu_a$ of the medium. After each scattering step, a new direction for the photon trajectory was calculated via the scattering phase function (the Henyey-Greenstein function [28]), which is specified by the anisotropy coefficient ($g$) of the tissue. The flight of the photon ended when it left the tissue (by crossing the tissue-air interface) or when its weight fell below a threshold minimum value (set to $1 \times 10^{-5}$), as determined by a Russian roulette routine [28]. At the end of its travel in the tissue, the time, $t$, spent by the photon within the medium was given by $t = L/nc$, where $L$ is the total

#69865 - $15.00 USD Received 10 April 2006; revised 24 May 2006; accepted 4 June 2006

path-length of the photon, $c$ is the speed of light in vacuum, and $n$ is the refractive index of the medium [29].

For the two-fluorophore AC tissue model studied here, the simulation supported tissue models containing $N_f = 2$ fluorophores (emitting at $N_f$ different wavelengths) that were considered to be uniformly distributed in the tissue medium [30]. The incident excitation could be absorbed by any one of the $N_f$ fluorophores. After each scattering event of the excitation photon, fluorescence absorption was sampled using a rejection technique, as governed by a cumulative fluorescence absorption coefficient $M_{af}$. Here, $M_{af}$ was the sum of the fluorescence absorption coefficients ($\mu_{afx}$) of all $N_f$ fluorophores specified in the tissue model, i.e. $M_{af} = \Sigma^i \mu_{afx}$ ($1 \leq i \leq N_f$). Once it was determined that the photon had been absorbed to produce a fluorescence photon, the wavelength of the remitted fluorescence photon was selected by a MC routine, where the probability of absorption of the excitation photon by one of the $N_f$ fluorophores was equal to the ratio ${}^i\mu_{afx} / M_{af}$ ($1 \leq i \leq N_f$) [30]. Upon successful fluorescence absorption, the excitation photon was relabeled a fluorescence photon, its new direction of travel was determined by an isotropic scattering event, and its weight was multiplied by the fluorescence quantum yield, ${}^i\Phi_{QY}$. This newly created fluorescence photon then continued to propagate from the point of its spatial origin (blue lines - collagen type II, red lines – NADH in Fig. 5), as governed by the scattering, absorption, and anisotropy coefficients of the medium at the fluorescence emission wavelength. After each successful fluorescence absorption event, the simulation added a sampled decay time, $t_d$, to the photon's total time of flight to include the effect of a finite fluorophore lifetime ($\tau_0$).

To simulate the experimental procedure of placing the fiber probe (see Fig. 2) above the AC sample surface, the reflectance and fluorescence photons were collected within an annulus of inner radius = 0.15 cm and outer radius = 0.33 cm (relative to source fiber center). The simulation required input values of $\mu_a$ and $\mu_s$, which were obtained from IS experimental measurements while the anisotropy was kept at a literature value of $g = 0.9$ [31], as described in Section 3.2. In this study separate codes were run for two fluorescence emission wavelengths (400 nm and 540 nm) to simulate experimental data. Wavelength dependence of fluorescence emission characteristics of the two fluorophores were introduced by using the spectrally weighted fluorescence emission $W(\lambda)$ described in Section 2.3 in lieu of the quantum yield coefficients ${}^i\Phi_{QY}$. The tissue thickness $z_1$ was the same as those for the samples

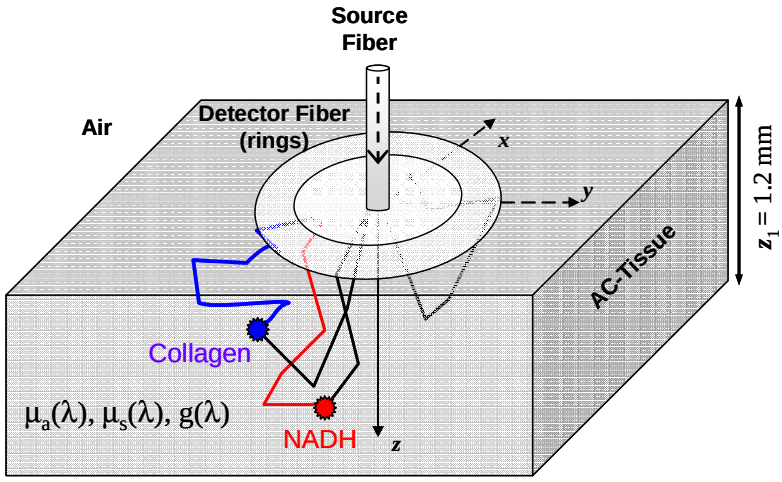


Fig. 5. Model for articular cartilage tissue showing fluorescence from two uniformly distributed fluorophores (intracellular NADH and extracellular collagen) relative to the excitation-detection fiber probes, as simulated by the MC code.

used in Section 2.4. Fluorophore lifetime for bound NADH was set to 1.5 ns [10,19]. The input values for the fluorescence lifetime of collagen and the relative fluorophore absorption

#69865 - $15.00 USD Received 10 April 2006; revised 24 May 2006; accepted 4 June 2006

coefficients ${}^{i}\mu_{afx}$ (for Collagen and NADH) were matched to simulate experimental measurements (described in Section 3.4).

Table 1. Scattering and absorption coefficients for AC tissue ($g$ = 0.9)

| Wavelength (nm) | $\mu_a$ (cm$^{-1}$) | $\mu_s$ (cm$^{-1}$) |
|---|---|---|
| 400 | 0.50 ± 0.05 | 300 ± 75 |
| 420 | 0.56 ± 0.02 | 285 ± 57 |
| 460 | 0.45 ± 0.16 | 220 ± 61 |
| 480 | 0.47 ± 0.09 | 188 ± 48 |
| 500 | 0.44 ± 0.23 | 168 ± 46 |
| 520 | 0.65 ± 0.06 | 133 ± 67 |
| 540 | 0.46 ± 0.21 | 199 ± 32 |
| 560 | 0.49 ± 0.21 | 125 ± 27 |
| 600 | 0.50 ± 0.20 | 106 ± 20 |

## 3. Results and discussion

### *3.1 Fluorescence excitation-emission matrix (EEM)*

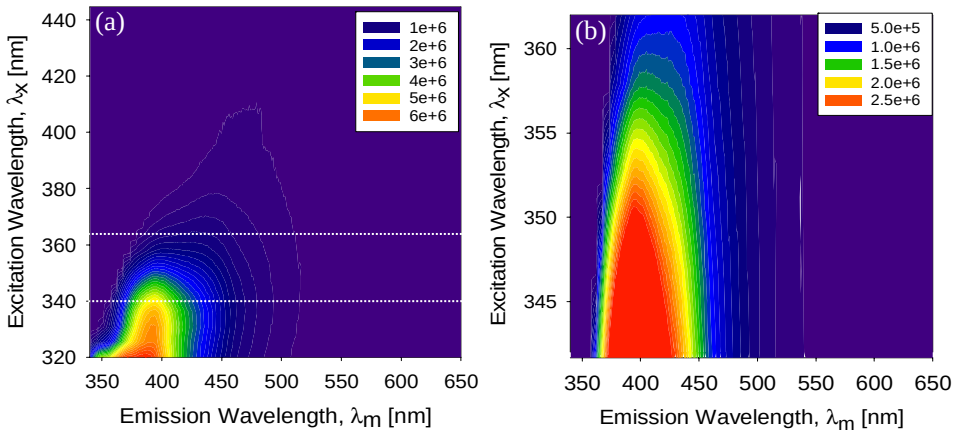


Fig. 6. (a) Measured EEM of articular cartilage (AC) tissue showing fluorescence emission primarily associated with extracellular collagen and intracellular NADH. (b) Same EEM expanded to highlight the area between white dotted lines in (a). RFLS excitation occurred at 355 nm. The EEM data was measured on the Fluorolog-3 spectrofluorometer.

Figure 6(a) shows EEM data for AC tissue sample #12. The EEM fluorescence intensity pattern was consistent with endogenous tissue fluorescence from extracellular collagen and intracellular NADH [2-5,7,16,32]. Figure 6(b) shows this EEM data around excitation wavelength 355 nm, which was the wavelength employed for excitation in RFLS studies. These EEM tissue data were consistent with measurements on pure collagen and NADH at 355 nm excitation (Fig. 3), further confirming the hypothesis that these two fluorophores represent the primary components of AC tissue autofluorescence in RFLS studies. Thus, the AC tissue model developed for computational simulations of these measurements was composed of these two endogenous tissue fluorophores.

### *3.2 Porcine AC tissue optical coefficients*

AC Tissue optical absorption ($\mu_a$) and scattering ($\mu_s$) coefficients at nine wavelengths were calculated from IS measurements by employing the IAD software and an anisotropy value of

#69865 - $15.00 USD Received 10 April 2006; revised 24 May 2006; accepted 4 June 2006

$g$ = 0.9 [31] (Table 1). For each coefficient, the table lists the mean ± standard deviation over data obtained on two AC tissue samples. The $\mu_s$ values decreased with increasing wavelength indicating lower wavelengths were scattered more by the tissue. There was no such specific trend for $\mu_a$ values. MC simulations were run using the two sets of $\mu_a$ and $\mu_s$ that were calculated using data from both tissue samples.

### *3.3 Reflectance spectroscopy: experimental measurements and computational modeling*

Reflectance from 11 AC tissue samples (samples # 1-11, Table 2) varied over the wavelength spectrum and increased between 400 nm and 540 nm. The gray line in Fig. 7 shows the measured average normalized reflectance as a function of wavelength between 400 and 600 nm. The normalization procedure set the reflectance at 540 nm to unity. Table 2 lists details of sample preparation for all samples, as well as the percentage increase ($\Delta R$), in reflectance at 540 nm ($R_{540}$) vs. reflectance at 400 nm ($R_{400}$). Thus, $\Delta R = [R_{540} - R_{400}]*100/ (R_{540})$. The average measured $\Delta R$ value was found to be 23 (±7) %.

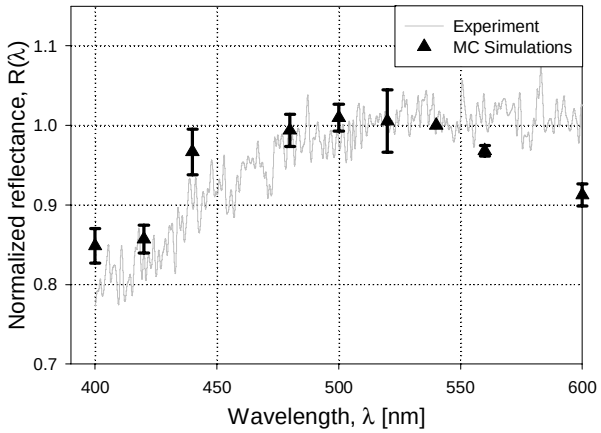


Fig. 7. Average, measured (gray, solid line) and simulated (black, triangles) normalized reflectance spectra from porcine AC. The normalization was done by setting reflectance at 540 nm to unity. The model inputs at each indicated wavelength were obtained from integrating sphere measurements. The error bars represent the results of the variations in the optical properties (see Table 1) input to produce the simulations.

A set of nine simulations were run to study the radially resolved reflectance at nine excitation wavelengths between 400-600 nm (listed in Table 1). At each wavelength, two simulations were run using two sets of $\mu_a$ and $\mu_s$ values, obtained as described in Section 3.2. Figure 7 shows mean normalized reflectance (black triangles) calculated by the MC simulations. The error bars represent the standard deviation between outcomes at each wavelength. The MC simulation predictions matched the average experimental data to better than 11% over the entire spectral range and predicted a $\Delta R$ of 15 (±2) %. This corroboration between experiment and simulation for reflectance gave us confidence in our estimation of the wavelength dependence of the tissue optical properties of porcine AC. A similar study has been done to assess bovine cartilage thickness using MC simulations [33]. This study did not consider any wavelength dependence of the absorption and scattering coefficients.

### *3.4 Fluorescence and fluorescence lifetime spectroscopy: experimental measurements and computational modeling*

Figure 8(a) shows a representative normalized intrinsic fluorescence spectrum from (sample # 15, Table 2) porcine knee AC tissue measured using the RFLS (black line). The fluorescence emission peaked near 400 nm, and was attributed to collagen dominated emission. The measured average decay time for the entire spectrum (i.e. with no BP filter employed) was observed to be 5.4 ± 0.5 ns, which was consistent with collagen dominated emission [34].

#69865 - $15.00 USD Received 10 April 2006; revised 24 May 2006; accepted 4 June 2006

Figure 8(a) also shows the band-pass filters centered at 400 nm (dashed blue box) and at 540 nm (dashed red box), employed to take time-resolved measurements as described in Section 2.3. These representative, normalized time-resolved data obtained from the same AC tissue (sample # 15, Table 2) are shown in Fig. 8(b) for the BP at 400 nm (solid blue line) and for BP at 540 nm (dashed red line). The dotted black line in Fig. 8(b) shows the temporal profile of the excitation laser pulse. As can be seen in Fig. 8(b), the blue curve (BP 400) decayed slower than the red curve (BP 540). This trend was seen consistently amongst all the 15 measured samples (Table 2). A one sided, unequal variances, Student t-test for the mean values of decay time at 400 nm and 540 nm wavelengths, yielded a P-value of $1.21 \times 10^{-5}$, indicating that the mean decay times were different from each other at the two band-pass filter locations.

As mentioned earlier, collagen type II and NADH were considered to be the two major fluorophores in the porcine AC tissue sample. The time-resolved fluorescence decays from each AC tissue sample at the two emission wavelengths (with BP filters centered at 400 nm and 540 nm) were simulated via two different tissue models to account for the differences in the optical transport coefficients at these two wavelengths. These simulated decays were analyzed by a bi-exponential model and an average decay time parameter was determined [19]. For each tissue model the tissue optical transport coefficients required at the central wavelength of each BP were obtained from the IS measurements as discussed in Section 3.2 (Table 1). The spectrally weighted fluorescence emission $W(\lambda)$ (Fig. 3) at the corresponding central wavelength of the BP filter were used in lieu of the fluorophore quantum yields. These spectrally weighted fluorescence emission coefficients were $1.35 \times 10^{-3}$ and $1.35 \times 10^{-5}$, for collagen and NADH, respectively, for the 400 nm BP tissue model while at 540 nm they were $8.64 \times 10^{-5}$ and $2.80 \times 10^{-4}$ for collagen and NADH, respectively.

Given these inputs for the fluorophore quantum yield coefficients, the simulations predicted that average decay time for the fluorescence signal at 400 nm using the bi-exponential model collapsed to the original input lifetime of collagen in the tissue model

Table 2. Porcine articular cartilage (AC) sample preparation, experimental and, computational results.

| AC Tissue Sample # | Sample Preparation | Measured $\Delta R^{\$}$ | Measured average fluorescence decay time (ns) | | Simulated fluorescence decay time (ns) at BP 540 nm | Extracted $\eta^{\%}$ |
|---|---|---|---|---|---|---|
| | | | BP[!] 400 nm | BP 540 nm | | |
| 1 | Freshly harvested | 25 % | 4.3 | 4.0 | 4.04 | 25.00 |
| 2 | Freshly harvested | 17 % | 5.4 | 5.3 | 5.25 | 60.00 |
| 3 | Freshly harvested | 29 % | 4.8 | 4.1 | 4.13 | 12.00 |
| 4 | Freshly harvested | 22 % | 4.9 | 4.1 | 4.13 | 10.54 |
| 5 | Freshly harvested | 11 % | 5.1 | 4.5 | 4.49 | 15.00 |
| 6 | Cultured* | 28 % | 5.4 | 4.0 | 3.98 | 5.45 |
| 7 | Cultured* | 28 % | 5.3 | 4.8 | 4.81 | 20.33 |
| 8 | Cultured | 22 % | 5.2 | 4.6 | 4.60 | 16.00 |
| 9 | Cultured | 13 % | 5.1 | 4.0 | 4.00 | 7.00 |
| 10 | Cultured | 29 % | 5.1 | 4.6 | 4.59 | 18.53 |
| 11 | Cultured | 27 % | 5.2 | 4.4 | 4.42 | 11.50 |
| 12 | Freshly harvested | - | 5.2 | 4.2 | 4.21 | 8.52 |
| 13 | Freshly harvested | - | 5.3 | 4.2 | 4.21 | 7.59 |
| 14 | Cultured | - | 6.4 | 3.0 | 3.00 | 1.38 |
| 15 | Freshly harvested | - | 5.1 | 4.5 | 4.49 | 15.00 |
| | *Average value* | *23± 7 %* | *5.2 ±0.4* | *4.3±0.5* | | |

* Measurements taken on different sites of an elongated tissue sample.
$ $\Delta R$ = percentage increase in reflectance at 540 nm ($R_{540}$) vs. reflectance at 400 nm ($R_{400}$)
! BP = band-pass filter
% $\eta$ = ratio of the fluorescence absorption coefficients of collagen to NADH (see section 3.4)

#69865 - $15.00 USD Received 10 April 2006; revised 24 May 2006; accepted 4 June 2006

(irrespective of the exact values of the lifetimes of either fluorophore), if ($\eta$) the ratio of the fluorophore absorption coefficient of collagen to that of NADH was greater than 0.1, which included the most physically plausible values for these fluorophores [19]. This behavior was anticipated in these simulations, since the weight of remitted fluorescence photons from collagen was on average 100 (approximately the ratio of the $W(\lambda)$ inputs of collagen to NADH at 400 nm) times larger than weight of remitted fluorescence photons from NADH. This result, however, meant, that each measured average decay time with the 400 nm BP filter would have to be interpreted as the lifetime of collagen for each particular sample. The variability seen amongst samples could be attributed to changes in the environment of the fluorophore.

Hence, in the 540 BP tissue model, for each sample, the input lifetime of collagen was set to the average decay time measured (for the same sample) via the 400 nm BP while holding the lifetime of NADH at 1.5 ns. The model was then used to extract the fluorescence absorption coefficients ($\mu_{afx}$) of both fluorophores by matching (to within 1%) the simulated average decay time at 540 nm to the experimentally measured fluorescence decay time

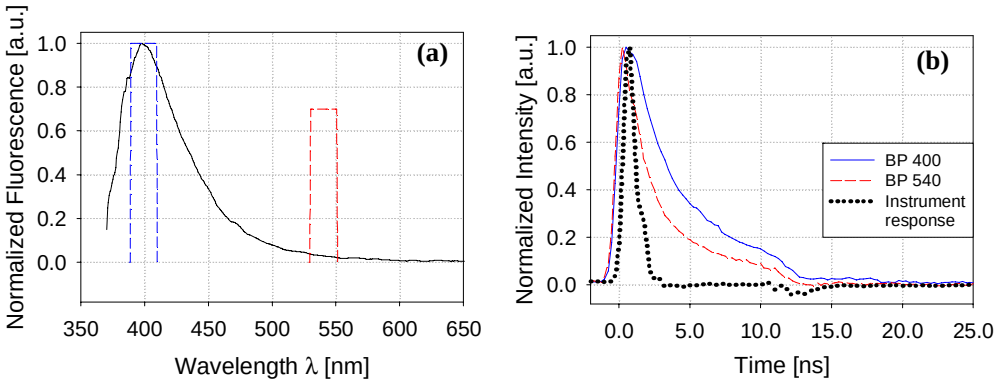


Fig. 8. (a) Autofluorescence spectrum of AC tissue (black line) acquired on the RFLS. Blue and red boxes indicate band-pass (BP) filters placed at 400 and 540 nm to measure fluorescence decay times for photons from those parts of the spectrum. (b) Time-resolved fluorescence of the tissue with a BP filter of 400 nm (solid blue line) and a BP filter of 540 nm (dashed red line). The black dotted line shows the excitation pulse temporal profile (instrument response).

measured via the 540 nm BP. Table 2 shows the values for $\eta$, the ratio of the fluorescence absorption coefficient of collagen to that of NADH for each measured AC tissue sample. Also shown are the predicted values of the simulated decay times using the $\eta$ values specified. The extracted $\eta$ values were found to vary by a large amount. One source of this variation could be the high variability in biological samples which can not be accounted for by simulations. It is thought that by repeating this study for a large number of samples the expected range of $\eta$ values for naturally occurring AC tissues could be extracted. Then comparison of $\eta$ values for artificially constructed AC tissue with this range could serve as a check of the viability of the construct. In addition, this method of extracting $\eta$ values could be used to monitor the development of an AC tissue construct over time, in a non-invasive manner.

Previous fluorescence lifetime imaging studies of what appear to be fixed and sectioned slices of porcine AC did not explain the biological origins of the detected fluorescence nor the statistical significance of the obtained data [35].

## 4. Summary and conclusion

In conclusion, a method for noninvasive, quantitative characterization of fresh tissues using reflectance and fluorescence measurements was applied to porcine knee AC. To the best of our knowledge, the work described in this report is the first study of endogenous fluorescence

#69865 - $15.00 USD Received 10 April 2006; revised 24 May 2006; accepted 4 June 2006

from unfixed and untreated porcine knee AC, where the biological origins of the measured fluorescence and reflectance are explained in the context of a quantitative model for photon transport in AC tissue.

MC simulations of photon propagation in a single layer, two – fluorophore (extracellular collagen type II and cellular NADH) tissue model were used to quantitatively explain experimentally measured fluorescence and reflectance signals from AC tissue. The concept of a spectrally weighted fluorescence emission $W(\lambda)$ was introduced to account for the wavelength dependence of fluorescence emission characteristics of the two fluorophores. The experimental and computational results agreed to within 11% of the mean reflectance spectra (from 11 samples), which provided the wavelength dependent tissue optical properties ($\mu_a$ and $\mu_s$) for porcine AC tissue models. For fluorescence measurements, a combination of experimental measurements and computational simulation was used to extract a quantitative description of the samples. For each AC tissue sample, the MC simulations for fluorescence used the measured decay time at BP 400 nm as an input to extract the ratio of fluorescence absorption coefficients ($\eta$) of the constituent fluorophores such that simulated average decay time at 540 nm were made to match to within 1%, the experimentally measured fluorescence decay time.

Although the AC tissue models used the optical transport coefficients determined via the IS-estimated average, it is to be noted that the reflectance spectrum from each sample could be inverted via MC simulations (guided by the IS values) to obtain the sample's transport coefficients. Estimation of $\mu_a$ and $\mu_s$ using MC simulations vs. IS, for tissue models that had identical $\eta$ values but modeled extreme variations of the transport coefficients, yielded average decay times (at 540 nm) that were within 1% of the decay time determined via using the IS estimates.

The approach presented here attributes a single fluorescence decay time to each constituent fluorophore in a tissue. A further refinement to this approach could include changes in fluorophore lifetime with emission wavelength. Although future systematic studies on pure substances should resolve conflicting reports existing in the literature regarding lifetime variations with wavelength (for example, for collagen [34]), it remains problematic to use data acquired on pure substances to describe those molecules in complex environments, such as biological tissues. An alternate and more biologically relevant approach would be to employ optical molecular imaging (via, e.g., fluorescence lifetime imaging microscopy) to characterize spatially-resolved endogenous fluorophores in their tissue environment. These studies are ongoing and should prove useful to enhance the ability to quantitatively interpret experimental measurements on tissues.

Hyaline AC is found in the synovial joints and is an important contributor to the functional capacities of these joints. If a chondral defect or lesion occurs, it does not heal on its own. Thus methods are being developed to make tissue constructs that would mimic true AC. Pre- and post implantation testing of the viability of these constructs can potentially be done by analyzing the optical signal from them. Towards this goal, a first step has been taken to optically characterize porcine knee AC. This work and the methods developed here should aid in the future study of AC tissue constructs. For example, monitoring the change in $\eta$ value for a sample over time would help detect changes in the sample's biological make-up by giving a measure of changes in relative concentrations of the constituent fluorophores. Furthermore, since the method would be non-destructive, it would allow repeated assessment of a given sample over time to follow intervention, thereby significantly speeding up lengthy and expensive protocols requiring multiple samples.

**Acknowledgments**

We thank Michael R. Francis at the Department of Biomedical Engineering, University of Michigan for his technical support. This research was supported by a grant from the National Institutes of Health NIH RR-020214 (to M.-A.M. and S.J.H.).

#69865 - $15.00 USD Received 10 April 2006; revised 24 May 2006; accepted 4 June 2006